Journal of Alloys and Compounds 509 (2011) 7961–7967

Contents lists available at ScienceDirect

Journal of Alloys and Compounds

journal homepage: www.elsevier.com/locate/jallcom

# EDX and ion beam treatment studies of filamentary in situ $MgB_2$ wires with Ti barrier

A. Rosova*, P. Kovac, I. Husek, L. Kopera

*Institute of Electrical Engineering, Slovak Academy of Sciences, Dúbravska cesta 9, 841 04 Bratislava, Slovakia*

ARTICLE INFO

*Article history:*
Received 19 April 2011
Received in revised form 11 May 2011
Accepted 13 May 2011
Available online 20 May 2011

*Keywords:*
Superconductors
Microstructure
EDS
SEM
Diffusion

ABSTRACT

In situ SiC-doped filamentary $MgB_2$ wires (with the diameter of 0.860 and 0.375 mm) with Cu stabilization separated by Ti barrier layers supported by outer SS sheath and annealed at 800 °C/0.5 h have been studied by combination of EDX analysis and ion beam selective etching. It was found that several Ti–Cu intermetallic compounds were created by Cu–Ti interdiffusion and thus the barrier protection against Cu penetration into the superconducting filaments is limited. We showed an advantage of Ti use as the barrier material in our wires. Ti getters silicon out from the superconducting filament, what purges superconducting $MgB_2$ from Si and creates an additional Si-rich layer in inner part of Ti barrier which prevents Cu diffusion more effectively.

© 2011 Elsevier B.V. All rights reserved.

## 1. Introduction

The choice of sheath material is crucial in ensuring the mechanical integrity in the fabrication of long length wires with high critical current while preserving chemical compatibility with $MgB_2$. The in situ reaction to form $MgB_2$ in iron or Nb sheath occurs usually at lower temperatures (600–750 °C) [1–3], which has the benefit of reducing undesirable interactions between the starting powders and the sheath material. However, improved $J_c$ values of in situ wires were obtained for $MgB_2$ wires using Ti diffusion barrier annealed at temperatures up to 900 °C indicating no detrimental chemical interactions [4–6]. Successful fabrication of 4-filament square in situ wires have been reported using Ti as a barrier layer in $MgB_2$/Ti/Cu/Monel with 10 wt% SiC in the core [5]. Effective Ti barrier must not only prevent the detrimental Cu diffusion into the filament and the formation of $MgCu_2$ [7], but the conductivity of the stabilizing Cu layer must also be maintained. The highest $J_c$ values in these wires are reported for reaction temperatures as high as 850 °C though the reaction layers at both $MgB_2$/Ti and Ti/Cu interfaces were detected by Vickers microhardness showing the correlation of interfacial reactions with increasing heat-treatment temperature [5]. Recently, 19 filaments in situ $MgB_2$/Ti/Cu/SS wires of 0.86 mm in diameter have been reported with the best performance after annealing at 800 °C/0.5 h [6]. In our previous work we have found decreasing critical current density of this wire type with reduced diameter especially for diameters smaller than 0.4 mm [8]. This $J_c$ degradation was attributed to thin Ti barrier (<10 μm), which is not able to protect $MgB_2$ filaments against the Cu penetration during annealing.

In this paper, an in-depth analysis of the microstructures of two wires with diameter of 0.860 and 0.375 mm heat treated (HT) at the same conditions (800 °C/0.5 h) is presented. Interfacial reaction layers and diffusion profiles were investigated using Energy Dispersive X-ray Spectroscopy (EDX). We exploited multiple facilities of Quanta 3D and relieved wire microstructure by ion beam preferential sputtering of wire cross-section surfaces.

## 2. Experimental

19-filament $MgB_2$/Ti/Cu/SS wires have been prepared by powder-in-tube process and in situ approach [6]. The composite wire contains: 50% of outer SS 316L reinforcement, 19.5% Cu stabilization, 19% Ti diffusion barrier and 8.5% $MgB_2$ filaments, see the insert in Fig. 1a. For improvement of in-field critical current density 5 wt% of SiC was added into a mixture of Mg and B powders [9,10]. Cold drawing deformation was applied from the composite wire diameters between 0.860 mm and 0.375 mm [8]. Short wire samples were heat treated at 800 °C/0.5 h in pure argon atmosphere. Critical currents ($I_c$ at 1 μV/cm) of heat treated wires were measured at liquid He temperature in external fields 3–8.5 T. $R(T)$ characteristics between 30 and 300 K have been also measured at self-field and in vacuum chamber using single stage cryocooler. Cross-sections of as-drawn 0.860 mm and heat treated (0.860 and 0.375 mm) wires were prepared by standard dry mechanical grinding and polishing. EDX mapping and analysis as well as Ga ion beam treatment of polished surfaces was performed by dual beam microscope FEI Quanta 200 3D.

* Corresponding author. Tel.: +421 2 5922 2311; fax: +421 2 5477 5816.
*E-mail address:* Alica.Rosova@savba.sk (A. Rosova).

0925-8388/$ – see front matter © 2011 Elsevier B.V. All rights reserved.
doi:10.1016/j.jallcom.2011.05.049

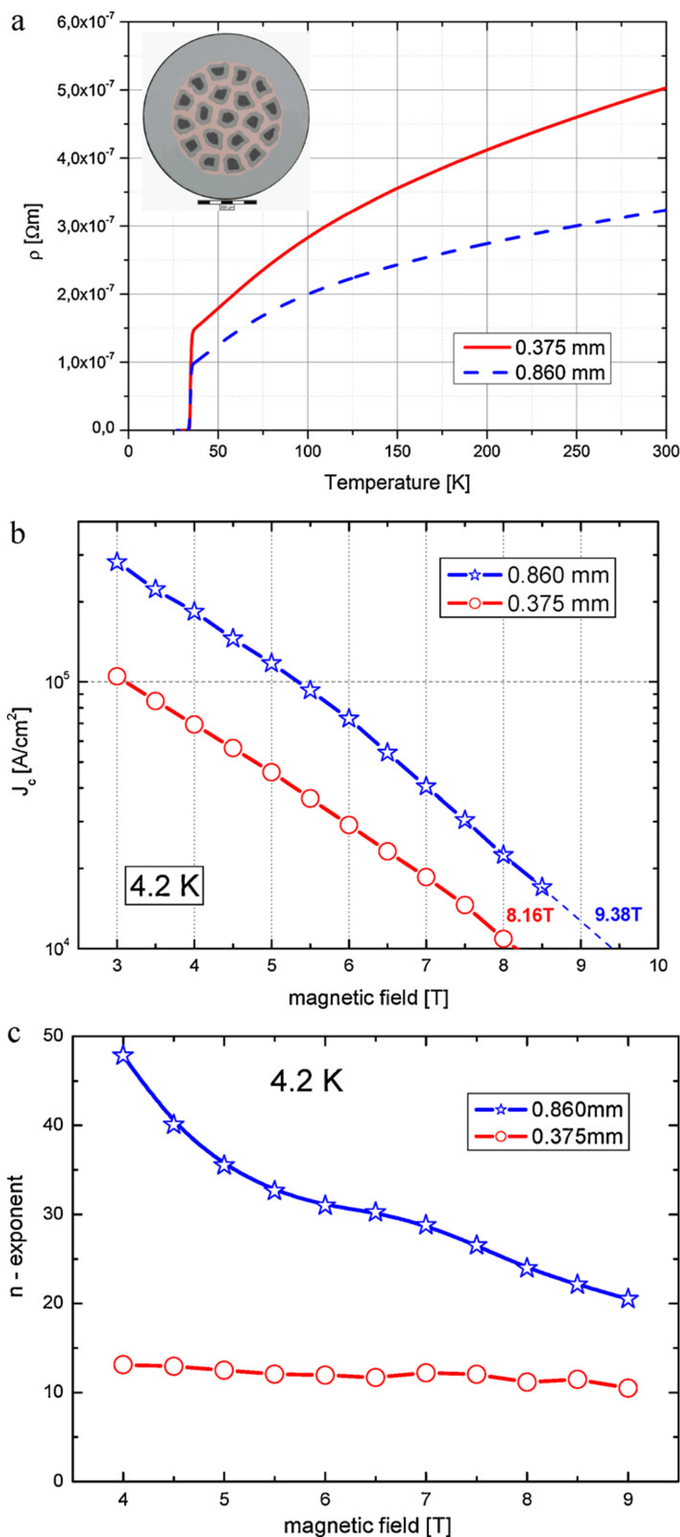


**Fig. 1.** Resistivities of wires 0.860 mm and 0.375 mm HT at 800 °C/0.5 h (a), the insert shows the cross-section of as-drawn Mg–B/Ti/Cu/SS wire of 0.86 mm. Critical current densities of wires 0.860 mm and 0.375 mm measured at liquid helium (b) and corresponding *n*-exponents derived from *I–V* characteristics (c).

## 3. Results and discussion

### 3.1. Electrical properties

Fig. 1a shows $\rho(T)$ characteristics of wires 0.860 mm and 0.375 mm annealed at the same conditions (800 °C/0.5 h). It is apparent that the resistivity of wire 0.375 mm is increased, what should be attributed to more intensive interface reaction in the less size wire (discussed in Sections 3.2.2 and 3.2.3).

**Table 1**
The main wire's dimensions measured before the final heat treatment.

| Wire diameter [mm] | Filament diameter [μm] | Ti barrier thickness [μm] |
|---|---|---|
| 0.860 | 58 | 22 |
| 0.375 | 25.7 | 9.6 |

Critical current densities of both wires at 4.2 K are plotted by Fig. 1b. Higher $J_c$ were obtained for 0.860 mm wire with 10,000 $Acm^{-2}$ in external field $B = 9.38$ T, while at 8.16 T for 0.375 mm wire. Similarly, the $n$ values of 0.860 mm wire are systematically higher than for 0.375 mm (see Fig. 1c), which reflects worse filament's quality and consequent transport current redistribution for thinner wire. The reduction of wire diameter (0.86 mm → 0.375 mm) leads to smaller filaments (58 μm → 25.7 μm) and also to thinner Ti barrier (see Table 1), which is not able to protect $MgB_2$ filaments against the Cu diffusion [8].

### 3.2. Elements distribution at wire's interfaces

#### 3.2.1. As-drawn wire 0.860 mm

No important reaction between the Ti barrier and adjacent sheath interfaces has been examined after mechanical stress exposition during drawing. Chemical element maps (Fig. 2b) as well as line scans (Fig. 3a) have simple structure corresponding to the filament geometry. As it is shown in Fig. 2a the Ti sheath interfaces have become ragged by multiple material deformations. This roughness influences partially the interface width reflected in the line scans. Together with applied experimental conditions (as e.g. a real dimensions of by electron beam excited volume during scanning and characteristic X-ray detection) it causes the vertical lines in element distribution dependence are not ideally vertical, but slightly inclined (Fig. 3a). Further spreading of interface in the line scans can be affected by mutual smearing of materials which have a tendency to galling as pure copper or titanium during cross-section sample polishing.

To avoid the effects of smeared surface as well as an upper thin amorphous layer created by mechanical polishing we used surface sputtering by scanning of focused gallium ion beam with energy of 30 keV. Because the sputtering yield depends strongly on the used material, its orientation and presence of structural defects, such "ion etching" is selective and it can relieve some microstructural inhomogeneities invisible in polished cross-section observations. Latter in Section 3.3 we extend a bit the discussion concerning the resulting surface pattern, which does not correspond directly to sample microstructure in simple way, but it can help to analyze material microstructure and visualize some features hidden under the polished surface. With circumspection in interpretation we can use ion beam in dual beam equipment as a tool of surface etching like metallographers use chemical etching to visualize microstructure for ages. Due to better achieved material contrast after the ion etching all SEM images presented in this article are taken after slight perpendicular ion beam etching (except if otherwise stated).

The same ion beam treatment was used for the cross-section surface of wire 0.86 mm illustrated in Fig. 4. It is a detailed SEM image showing Ti barrier part close to the outer stainless steel sheath. In addition we used a subsequent more intense sputtering of the strip part in the central part of the image using the perpendicular ion beam, too. Resulting surface profile illustrates more clearly no pre-reaction during drawing and visualize well the interfaces roughness.

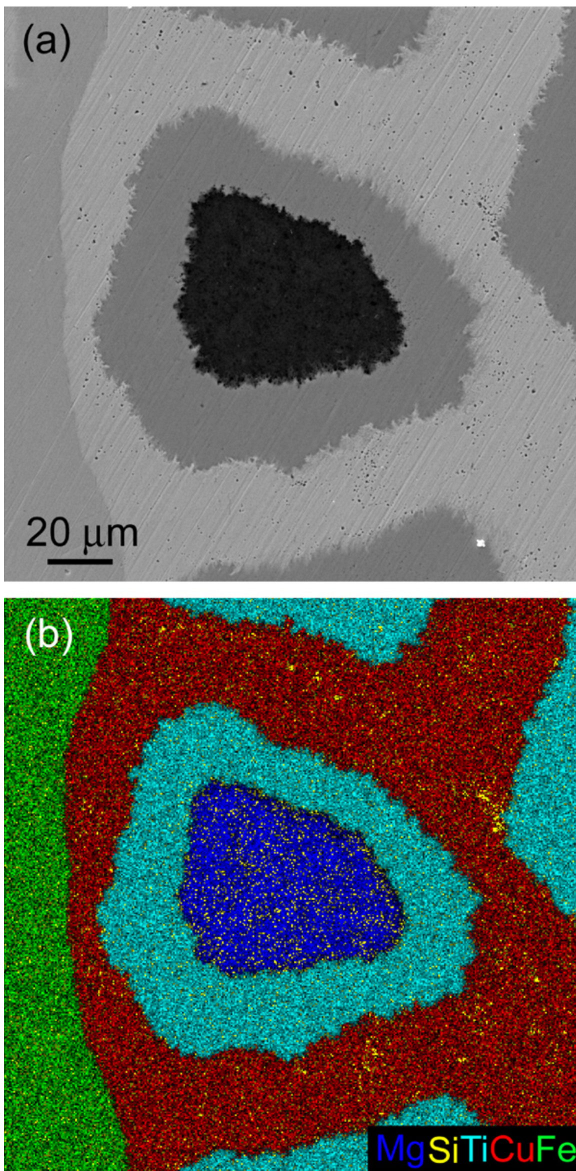


**Fig. 2.** SEM image (a) and chemical element map (b) of a filament area in as-drawn 0.860 mm wire.

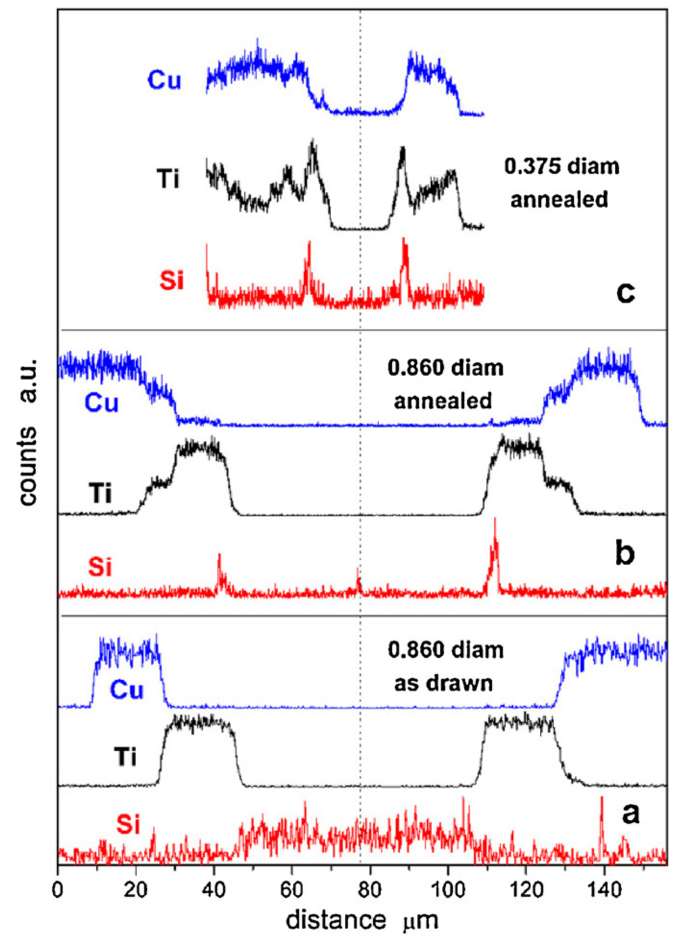


**Fig. 3.** Line scan profiles for the as-drawn 0.860 mm wire (a), the wire 0.860 mm HT at 800 °C/0.5 h (b) and the wire 0.375 mm HT at 800 °C/0.5 h (c).

### *3.2.2. Heat treated wire 0.860 mm*

The element map in Fig. 5b shows the distribution of chemical elements around one filament area close to the steel sheath of wire 0.860 mm HT at 800 °C/0.5 h.

One can see clearly an apparent interdiffusion between Ti barrier and Cu stabilization and also a localization of Si in a thin layer outside of the $MgB_2$ filament. Some Si agglomerates are located also in voids or surface imperfections what suggests they came there from the used polishing media (SiC). To be sure that Si layer near to $MgB_2$ core is not caused by polishing; we re-polished the sample surface by diamond films. Si particle localized on the surface imperfections nearly completely disappeared, but those located round the outer core interface stayed unchanged. The later silicon-rich layer originates in process of decomposition of SiC, which was used as a dopant in $MgB_2$ filaments. We suppose that during the heat treatment the carbon from decomposed SiC was built-in $MgB_2$ lattice [9–11] and Si originally spread over the whole Mg–B filament (see Figs. 2b and 3a) was gettered by titanium barrier out off the $MgB_2$. We note a decreased interfaces roughness in comparison to the as-drawn wire (see Section 3.2.1) after the heat treatment, too.

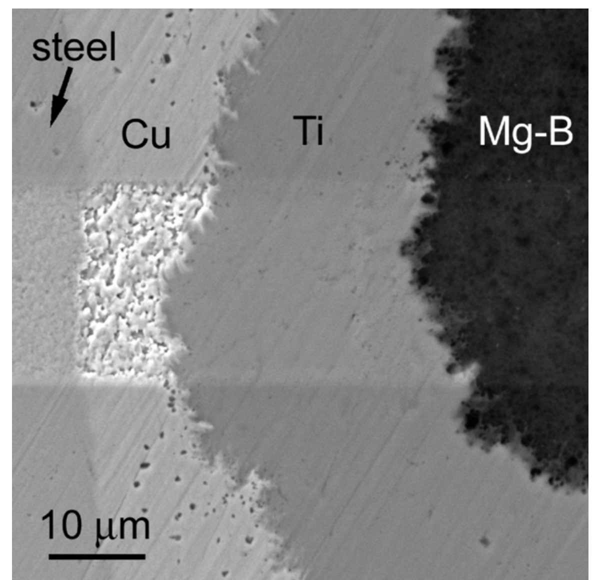


**Fig. 4.** SEM image of ion beam treated surface of polished cross-section of as-drawn 0.860 mm wire.

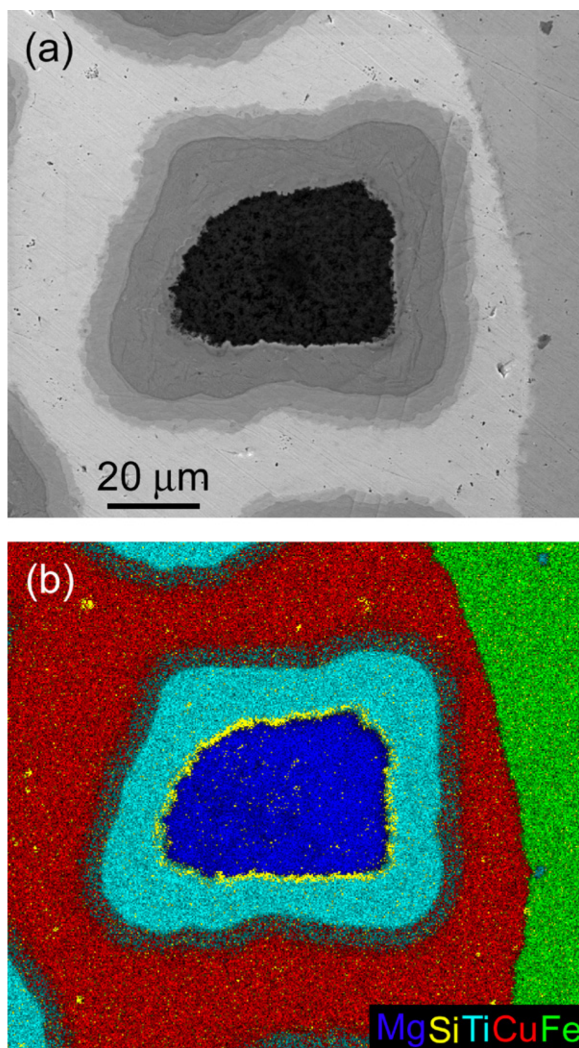


**Fig. 5.** SEM image (a) and chemical element map (b) of a filament of wire 0.860 mm HT at 800 °C/0.5 h.

In Fig. 3b there is a line scan made for the heat treated $MgB_2$ filament displayed in Fig. 5. Its step-like dependence shape reflects Ti–Cu interdiffusion. Moreover, the line-scan shows more precisely the location of Si at the inner side of Ti sub-layer surrounding $MgB_2$ filament. The thin maxima in Si line-scans in Fig. 3b correspond to location of pores on filament cross-section surface and they are also visualized as yellow spots in chemical element map in Fig. 5b. We suppose they originate in SiC contamination from wire cross-section polishing. The ion sputtering removed the surface SiC contamination, but it could not remove completely a rest of SiC from deeper pores.

In comparison to the non-annealed wire the content of Si in $MgB_2$ filament volume decreased in annealed wire. See also the values of Si content in the central zone of superconducting cores measured from the area cca 12 μm × 12 μm of all observed filaments summarized in Table 2. This is an important advantage of Ti

**Table 2**
Ratio of Mg, Ti, Cu and Si in the centre of $MgB_2$ filament (from the area of cca 12 μm × 12 μm) measured by EDX in atomic %.

| Analyzed sample | MgK | TiK | CuK | SiK |
|---|---|---|---|---|
| As-drawn 0.860 mm | 89 | 0 | 0 | 11 |
| HT 0.860 mm | 97 | 0 | 1 | 2 |
| HT 0.375 mm | 95 | 0 | 4 | 1 |

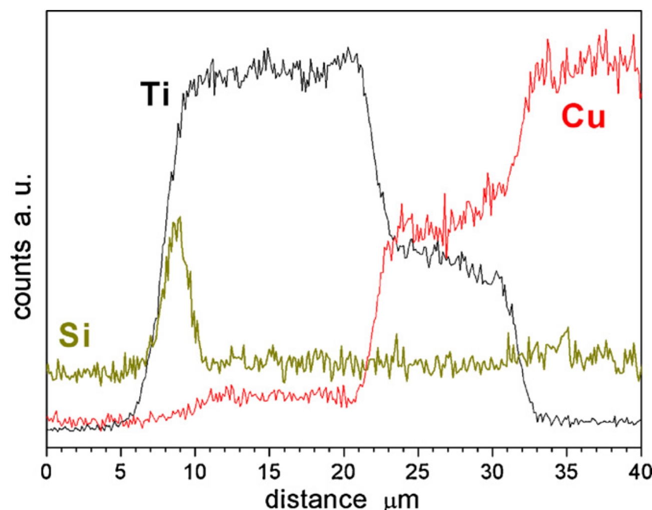


**Fig. 6.** Line scan of Ti barrier area of wire 0.860 mm HT at 800 °C/0.5 h.

sheath, because, as it is known from the Mg–Si phase diagram [12], Si can react with Mg to create $Mg_2Si$ phase even at relatively low temperatures. Thus increased Si content in the filament can result in a larger volume of non-superconducting secondary phase and in the same time decrease of Mg/B ratio. The presence of Si accumulated at grain boundaries can worsen substantially inter-grain connectivity, too [10].

Besides the big steps in the line scan in Fig. 3b their gradual intensity decreasing and increasing near to the step boundaries evokes possible existence of thin layers of different Cu/Ti ratio (see the line-scan of Ti barrier zone in Fig. 6). They were not visible on polished surface, but the ion etching pointed out their presence by increasing of their mutual contrast difference by damaged surface layer removing, preferential sputtering of different material and preferential sputtering of their boundaries. To simplify discussion we marked the recognized layers by numbers in Fig. 7.

Quantitative EDX analyses were made on polished or polished and slightly ion treated samples, because ion sputtering can change atomic ratio in alloys and fine-grained mixture of different phases due to its selectivity. We do not estimate content of light elements because of high experimental error caused not only by measure-

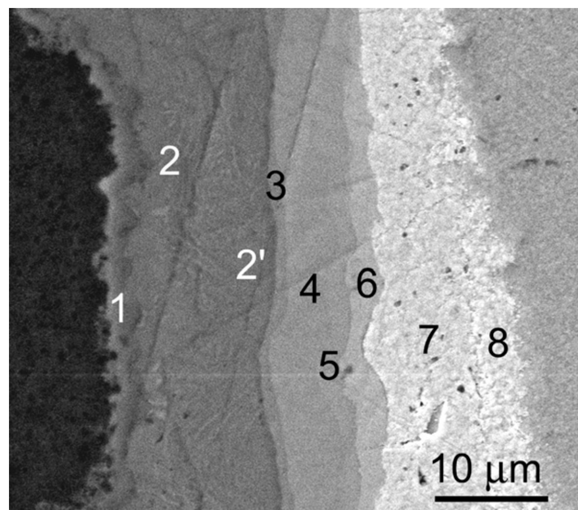


**Fig. 7.** SEM image of Ti barrier layered structure after HT at 800 °C/0.5 h. The surface was treated by slight sputtering by ion beam perpendicular to the sample surface.

**Table 3**
Ratio of Mg, Ti, Cu and Si in the $MgB_2$ filament and individual layers (marked by numbers in Fig. 7) measured by EDX in atomic %.

| Analyzed layer | MgK | TiK | CuK | SiK | Phase |
|---|---|---|---|---|---|
| $MgB_2$ | 97 | <1 | <1 | 2 | – |
| 1 | 6 | 85 | 0 | 9 | Ti (+Si, Mg) |
| 2 | 0 | 96 | 4 | 0 | Mixture of Ti |
| 2′ | 0 | 92 | 8 | 0 | and $Ti_2Cu$ |
| 3 | 0 | 70 | 30 | 0 | $Ti_2Cu$ [a] |
| 4 | 0 | 50 | 50 | 0 | TiCu |
| 5 | 0 | 43 | 57 | 0 | $Ti_3Cu_4$ |
| 6 | 0 | 21 | 79 | 0 | $TiCu_4$ |
| 7 | 0 | 3 | 97 | 0 | Cu (+Ti) |
| 8 | 0 | 8 [b] | 85 [b] | 0 | Cu (+Ti, Fe, Cr) |

[a] Higher difference from the expected value could be caused by small thickness and thickness inhomogeneity of the $Ti_2Cu$ layer.
[b] Content of Ti is variable (see text), here Ti:Cu:Fe:Cr = 8:85:5:2.

ment of light elements as a problem itself but also by different peak overlapping.

The ratios of Mg, Ti, Cu and Si content in atomic % in the individual layers marked according Fig. 7 are summarized in Table 3. The layered Ti–Cu part of wire can be expressed a sequence of layers: Ti contaminated by Si and Mg (1), mixture of Ti and $Ti_2Cu$ (2), $Ti_2Cu$ (3), TiCu (4), $Ti_3Cu_4$ (5), $TiCu_4$ (6), Cu contaminated by Ti (7). This result corresponds well to the sequence of solid phases in Cu–Ti system binary phase diagram [12] and results published on analysis of Cu–Ti laminated system annealed at 650 or 750 °C/1 h [13]. In comparison to the Ti–Cu phase diagram $Ti_2Cu_3$ is missing in our sequence, but it could be sheltered as undistinguished thin layer between the layers 5 ($Ti_3Cu_4$) and 6 ($TiCu_4$). The deviation of measured Cu:Ti ratio in the layer 6 in comparison to the theoretic ratio 20:80 for $TiCu_4$ could support this idea.

The thick layer 2 is composed of mixture of Ti and $Ti_2Cu$ with variable ratio of Ti to Cu content where ratio Ti/Cu decreases with increasing distance from the $MgB_2$ filament. Their microstructure is relieved by ion milling into two-levels-of-gray contrast (Fig. 7). The mixture of Ti and $Ti_2Cu$ is a result of eutectoid transformation and obviously has characteristic lamellar microstructure very similar to the observed contrast distribution [14].

In this way all former Ti sheath is changed by diffusion and no pure Ti rested. Nevertheless, the thin layer with higher Si content additionally constrain from Cu diffusion, what we consider as a further advantage of Ti sheath in case of core doping by SiC. The step in decreasing of Cu content is well visible in Fig. 6, too.

In areas with a small distance between Ti barrier and steel sheath where there is only a thin Cu layer between them we can see as titanium migrates through the thin Cu layer and it is accumulated on inner steel interface. Resulting Ti content located near the inner steel interface varies with Ti sheath distance from the interface. In the area in Fig. 7 where the Ti barrier is the closest to the steel sheath the content of accumulated Ti reaches the value of 8 at% in the alloy with content ratio Ti:Cu:Fe:Cr = 8:85:5:2. In this way Ti sheath in fine multifilament wires can be additionally locally thinned by removal of material from the sheath towards the steel outer cover. It is not so well visible on the map in Fig. 5, because the overlapping of different element contrast suppress faint Ti contrast in the vicinity of steel, but it is nicely visible in single Ti element map, which is not shown here. However, we can see clearly the result of this mechanism in the map of thinner wire after the same heat treatment in Fig. 8.

### 3.2.3. Heat treated wire 0.375 mm

To elucidate the situation when Ti barrier becomes too thin we analyzed diffusion profiles in a heat treated wire with diameter 0.375 mm, where mean thickness of Ti barrier before heat treatment was smaller than 10 μm (see Table 1). SEM images as well as chemical element maps show very intense and long distance Cu–Ti interdiffusion (Fig. 8). Ti and Cu are completely inter-diffused with variable atomic ratio. The thin layer surrounding $MgB_2$ filament containing the maximal concentrations of Ti and Si is the place of accumulation of silicon gettered from the filament. As it is visible from the corresponding line scan in Fig. 3c and Fig. 9, the Si-

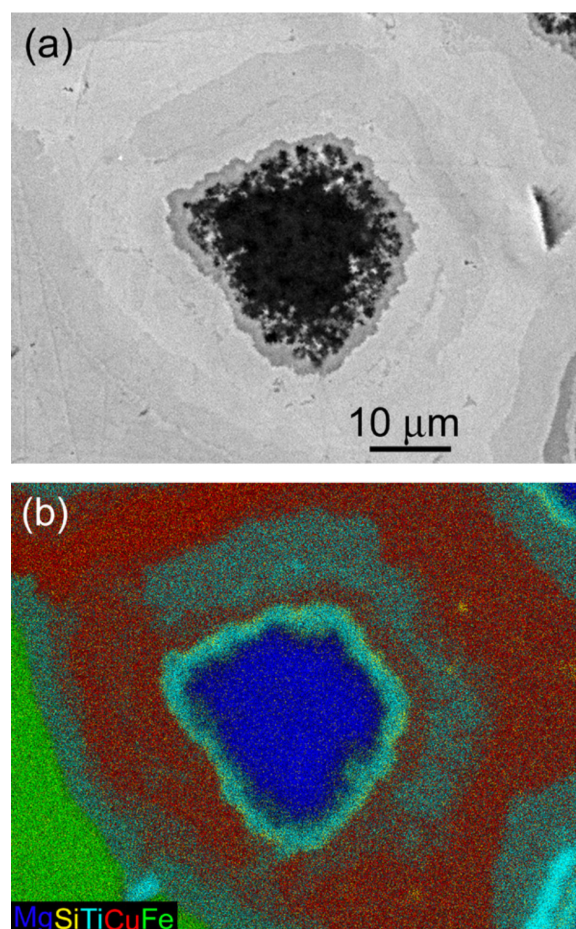


**Fig. 8.** SEM image (a) and corresponding element map (b) of a filament in wire 0.375 mm HT at 800 °C/0.5 h.

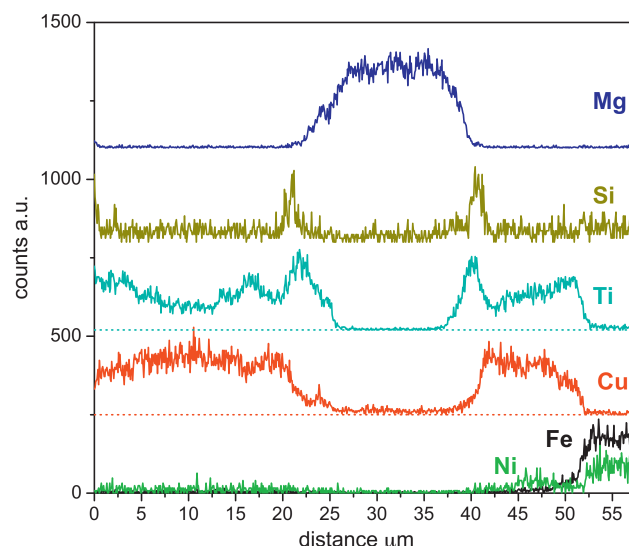


**Fig. 9.** Line scan of wire 0.375 mm HT at 800 °C/0.5 h.

rich layer can suppress Cu diffusion into $MgB_2$ filament, but cannot avoid it completely. Cu mixed with Ti penetrates into the filament creating islands of alloy decreasing the superconductor effective cross-section area (Fig. 8a). In the same time, Cu penetrates also into the $MgB_2$ (see the ratio of Cu content in the centre of the filament in Table 2) as impurity what decreases the superconductor quality. This explains well the decreased critical current density (Fig. 1b) as well as lowered *n*-exponent (Fig. 1c) for the 0.375 mm wire.

Higher resistivity of the thinner wire (Fig. 1a) is also influenced by huge diffusion after which well conductive Cu stabilization is transformed into alloy with higher resistivity. In addition, when thickness of Cu between filaments and steel sheath is decreased in 0.375 mm wire, due to proximity of the outer steel sheath an important mass of titanium was moved away to the inner steel interface, so the Ti sheath was additionally weakened from the outer side. As titanium reached the interface between steel and Cu stabilization matrix, it could react with steel elements and diffusion is increased in both directions (Fig. 9).

### 3.3. Ion beam surface treatment

We used ion beam sputtering of polished sample surface to increase the contrast between different phases and single out the presence of individual layers created during heat treatment. Obviously, ion etching is considered as a process influenced by too many parameters affecting the resulting sample topography, thus it is not regarded as sufficiently reliable in microstructure analysis. Really, many parameters connected with ion beam (as energy and type of ions, beam current, incident angle etc.), sputtered material (its density and chemical bonds, grain size and orientation, defect presence, sample temperature etc.) and even surface contamination influence sputtered surface profile by important way [e.g. 15–18]. A starting surface profile is also important due to angular dependence of sputtering yield.

In our dual beam equipment Quanta (and generally in comparable FIB equipment) $Ga^+$ ions with energies of about 5–30 keV are used. We scanned a treated surface with narrow beam with variable spot size and current and we can choose different angles of ion beam impingement. In addition we treat surface of complex material with alloys and compounds of variable grain size and composition. Due to character of our samples and their cross-section preparation we cannot ensure perfect cleanness and flatness of the surface. However, under all these parameters consideration we can reveal the samples microstructure invisible just after mechanical polishing of cross-section surface.

Firstly, the starting perpendicular ion beam sputtering removes thin upper amorphous layer caused by mechanical polishing. In this way the contrast between different materials becomes better. Consecutive removing of different materials with different sputtering rates causes creation of surface profile depending on material composition. In this way we were able to distinguish thin inter-layers caused by Cu–Ti diffusion, which were not visible after surface sample polishing and as well as more compact Ti + Si + Mg layer surrounding $MgB_2$ core (see layers 3, 5 and 6 in Fig. 7).

Further higher-dose sputtering by inclined ion beam gave rise to markedly different surface profiles for individual layers; see the strip in central zone of Fig. 10, which was sputtered by ion beam declined from the surface normal by 52° in the observer view direction. It is known that selective sputtering becomes more selective with higher incident angle measured from surface normal (with the maximum at about 80°) [15]. In this way the boundaries between the thin layers were transformed to surface steps and some Cu precipitates in the layers 5 ($Ti_3Cu_4$) and 6 ($TiCu_4$) were disclosed.

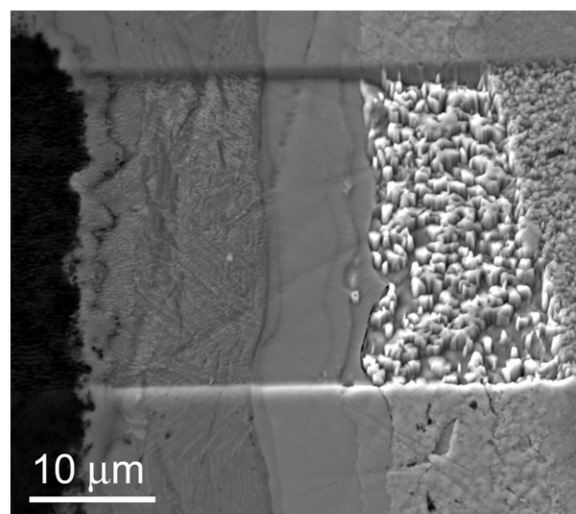


**Fig. 10.** SEM image of Ti barrier layered structure in the wire 0.860 mm HT at 800 °C/0.5 h. The surface was treated by slight sputtering by ion beam perpendicular to the sample surface and the central zone of the image was consequently sputtered by ion beam declined by 52° in direction of observer view.

On the other side inclined sputtering at lower temperatures and higher ion fluxes brings about surface modulations caused by competitive kinetic processes on the surface during ion sputtering [17,18]. They should be considered during surface profile interpretation to avoid mistakes. In our case the added rippled surface complicates interpretation of lamellar microstructure of the mixture of Ti and $Ti_2Cu$ (layer 2) as well as $MgB_2$ filament microstructure (Fig. 11). In the later case regular hills do not correspond to grains and sputtering under such conditions can show out only presence of voids (marked by arrows).

In Cu area very distinct cones appeared on the surface, what is a characteristic ion beam sputtering artifact for metals with surface impurities of metals with higher melting temperature [19]. Pure copper has melting point of 1085 °C and there are several possible impurities composed by Ti, Si or elements originating in steel outer cover with higher melting temperature in the wires.

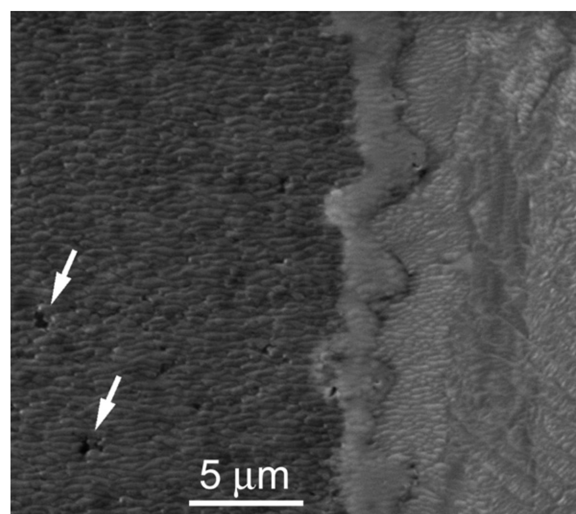


**Fig. 11.** SEM image of boundary zone of $MgB_2$ filament and Ti barrier in the wire 0.860 mm HT at 800 °C/0.5 h. The surface was treated by slight sputtering by ion beam perpendicular to the sample surface and consequently sputtered by ion beam declined by 52° in direction of observer view.

## 4. Conclusions

Considering all mentioned advantages and disadvantages of Ti as a barrier in in situ technology of fine-filament superconducting wires we can conclude titanium is a suitable sheath material in $MgB_2$ (SiC)/Ti/Cu/SS system. Even if Ti is not an "ideal" diffusion barrier that can avoid diffusion of Cu into $MgB_2$ filaments completely, it can protect the superconductor by Cu diffusion decelerating. The inter-diffused barrier volume after heat treatment is divided into several thin layers of different phases with multiple phase boundaries perpendicular to diffusion gradient and different resistance to Cu diffusion through the barrier. This imposes limits to the annealing temperature, time and especially the barrier thickness in fine filamentary wires.

A coexistence of Ti sheath with SiC as superconducting core dopant was also proved as advantageous. On one side Ti getters out Si from $MgB_2$ filament after SiC decomposition and in this way it prevents creation of non-superconducting parasite phase and worsening of inter-grain connectivity. On the other side Si accumulated in thin Ti layer located around the superconducting filaments helps to protect it from undesirable Cu penetration.

Grace of these features we could obtain good quality $MgB_2$ fine filament wires with high current densities in magnetic field.

We showed how ion sputtering of sample surface can help to detect some finer microstructural features invisible under as-polished material surface and in what way it can cause misinterpretations if the effect of surface ion beam modifications are not carefully considered.

## Acknowledgements

This contribution/publication is the result of the project implementation: Development of the Centre of Excellence for New Technologies in Electrical Engineering – 2nd stage, ITMS code 26240120019, supported by the Research & Development Operational Programme funded by the ERDF. This work was also supported by the Slovak Scientific Agency under the project APVV-0398-07 and VEGA 2/0037/09.

## References


[1] S.X. Dou, J. Horvat, S. Soltanian, X.L. Wang, M.J. Qin, S.H. Zhou, H.K. Liu, P.G. Munroe, IEEE Trans. Appl. Supercond. 13 (2003) 3199.
[2] W. Goldacker, S.I. Schlachter, B. Obst, M. Eisterer, Supercond. Sci. Technol. 17 (2004) S490.
[3] M.D. Sumption, M. Bhatia, M. Rindfleisch, M. Tomsic, E.W. Collins, Supercond. Sci. Technol. 19 (2006) 155.
[4] M. Alessandrini, H. Fang, M. Hanna, P. Putman, Y.X. Zhou, K. Salama, Supercond. Sci. Technol. 19 (2006) 129.
[5] P. Kováč, I. Hušek, T. Melišek, T. Holúbek, Supercond. Sci. Technol. 20 (2007) 771.
[6] P. Kováč, I. Hušek, T. Melišek, L. Kopera, M. Reissner, Supercond. Sci. Technol. 23 (2010) 065010.
[7] G. Liang, H. Fang, D. Katz, Z. Tang, K. Salama, Phys. C 442 (2006) 113.
[8] P. Kováč, I. Hušek, A. Rosová, T. Melišek, L. Kopera, Supercond. Sci. Technol. 23 (2010) 105006.
[9] P. Kováč, I. Hušek, V. Skákalová, J. Meyer, E. Dobročka, M. Hirscher, S. Roth, Supercond. Sci. Technol. 20 (2007) 105.
[10] S.K. Chen, X. Xu, J.H. Kim, S.X. Dou, J.L. MacManus-Driscoll, Phys. C 470 (2010) 1211.
[11] R.J. Cava, H.W. Zandbergen, K. Inumaru, Phys. C 385 (2003) 8.
[12] Th.B. Massalski, H. Okamoto, P.R. Subramanian, L. Kacprzak (Eds.), Binary Alloy Phase Diagrams, second ed., ASM International, USA, 2001.
[13] B.S. Bokstein, V.I. Vnukov, E.V. Golosov, M.I. Karpov, Yu.R. Kolobov, D.A. Kolesnikov, V.P. Korzhov, A.O. Rodin, Russ. Phys. J. 52 (2009) 811.
[14] S.A. Souza, C.R.M. Afonso, P.L. Ferrandini, A.A. Coelho, R. Caram, Mater. Sci. Eng. C 29 (2009) 1023.
[15] B.I. Prenitzer, C.A. Urbanik-Shannon, L.A. Giannuzzi, S.R. Brown, R.B. Irwin, T.L. Shofner, F.A. Stevie, Microsc. Microanal. 9 (2003) 216.
[16] G. Carter, I.V. Katardjiev, M.J. Nobes, J.L. Whitton, Mater. Sci. Eng. 90 (1987) 21.
[17] E. Chason, W.L. Chan, Nucl. Instrum. Methods Phys. Res. B 256 (2007) 305.
[18] M.V. Ramana Murty, Surf. Sci. 500 (2002) 523.
[19] G.K. Wehner, J. Vac. Sci. Technol. A 3 (1985) 1821.